Acetylene used as a New Linker for Molecular Junctions in Phenylene-Ethynylene Oligomer Langmuir-Blodgett Films

Luz Marina Ballesteros[a,b], Santiago Martín[a,b,c], María Cristina Momblona[a,b,c], Santiago Marqués-González[d], María Carmen López[a,b], Richard J. Nichols[e], Paul J. Low[d], and Pilar Cea[a,b,c *]

[a] Departamento de Química Física, Facultad de Ciencias, Universidad de Zaragoza, 50009, Spain.

[b] Instituto de Nanociencia de Aragón (INA), Edificio i+d. Campus Rio Ebro, Universidad de Zaragoza, C/Mariano Esquillor, s/n, 50017 Zaragoza, Spain.

[c] Laboratorio de Microscopías Avanzadas (LMA) C/ Mariano Esquilor s/n Campus Rio Ebro, 50018, Zaragoza, Spain.

[d] Department of Chemistry, University of Durham, Durham DH1 3LE, United Kingdom.

[e] Department of Chemistry, University of Liverpool, Crown Street, Liverpool, L69 7ZD, United Kingdom.

* Corresponding author. Email: pilarcea@unizar.es

Abstract

Langmuir and Langmuir-Blodgett films have been fabricated from an acetylene-terminated phenylene-ethynylene oligomer, namely 4-((4-((4-ethynylphenyl)ethynyl)phenyl)ethynyl)benzoic acid (HOPEA). Characterization of the Langmuir film by surface pressure vs. area per molecule isotherms and Brewster angle microscopy reveal the formation of a high quality monolayer at the air-water interface. One layer Langmuir-Blodgett (LB) films were readily fabricated by the transfer of HOPEA Langmuir films onto solid substrates by the withdrawal of the substrate. The deposition mode was Z-type. Quartz crystal microbalance (QCM) experiments confirm the formation of directionally oriented, monolayer LB films, in which the HOPEA molecules are linked to the gold substrate by attachment through the acid group. The morphology of these films was analyzed by atomic force microscopy (AFM), which revealed an optimum transference surface pressure of 18 $mN \cdot m^{-1}$ for the formation of homogeneous films. Cyclic voltammetry also showed a significant blockage of gold electrodes covered by HOPEA monolayers. Electrical properties of HOPEA monolayers sandwiched between a bottom gold electrode and a gold STM (scanning tunnelling microscope) tip have been recorded, revealing that the acetylene group is an efficient linker for electron transport. In addition, the STM experiments indicate a non-resonant tunnelling mechanism of charge transport through these metal-molecule-metal junctions.

Key words: Langmuir-Blodgett films; acetylene group; molecular junction; STM

Introduction

The design of molecules for use in molecular electronics has been a topic of intense interest since the seminal work of Aviram and Ratner.[1] The special roles of saturated, conjugated and redox active moieties within a molecular backbone have been elucidated and combined with various donor and acceptor groups to create a substantial library of molecular components with functions that range from simple wires to rectifiers, transistors and even logic elements.[2-6] In recent years, anchoring groups and electrode materials in molecular electronic junctions have also begun to receive special attention following the wide-spread recogniton that these factors can also strongly influence the charge transport characteristics of a molecular junctions.[7-12] Effective molecule-to-electrode contacts have been in particular focus in recent years, especially owing to the interest in single molecule junctions and growing capacity for single molecular electrical measurements.[13] In this regard, the exploration of different molecule-metal contacts is of current interest in order to determine the role of this interface in measurements of conductance of single molecules or molecular assemblies.[14-18] Thiol functional groups are most commonly used to contact organic compounds to gold to form an electrical contact.[19] Using thiol contacts it is possible to fabricate large area metal|molecule|metal junctions or even junctions in which a single molecule spans between a pair of metal contacts. At present, the drawbacks of thiol contacts to gold for fabricating reliable metal|molecule|metal junctions, such as surface etching, molecular mobility on the surface and high contact resistance are clearly apparent.[20-22] As a result other chemisorption chemistries using amines, carboxylic acids, nitriles etc. have also been employed to contact molecules to metallic substrates.[7,16,17,23-27] Recently, a new type of organic-metal contact has been reported, in which the phenyl terminal of an oligophenyleneethynylene monothiol is directly contacted to one of the gold contacts in a two-terminal configuration, the other contact being made through conventional thiolate-gold chemisorption.[11,28] These studies have concluded that the phenyl group contacts the electrode face-on through the end phenyl group to a gold adatom or other coordinated gold surface atom (referred to as a "high coordination site") leading to effective electrical junctions. This result opens new questions about how other π-rich terminal groups might also be employed for contacting single molecules or assembles of molecules at such defect sites on metallic electrodes. In this context, it seems that an

acetylenic moiety, –C≡CH, could also behave as a contacting group. Terminal acetylenes RC≡CH are synthetically available offering a cylindrical π-electron system that can be conjugated with the π-system of the molecular wire. Coordination of metal atoms and clusters to acetylenic-systems is well-known,[29,30] and acetylenes have a rich surface chemistry.[31] As junction components, acetylene moieties have also been covalently attached to hydrogen passivated silicon surfaces via surface based hydrosilylayion reactions[32] and can be used as reactive entities to further modify molecular species within the junction by facile click chemistry methods.[33]

Conductance studies for molecular assemblies often focus on 'symmetric' molecular junctions, where the respective chemical contacting groups at either end of the molecule binding to the electrode surfaces are identical. However, systems where the contacting groups at either ends of the molecule are different are also of interest, particularly since they may be used to promote efficient contact to different electrode materials. Non-symmetric molecular junctions, where there is a directional orientation of molecules between pairs of non-similar electrodes also have interest and can show rectifying or diode-like behaviour.[16,17,34,35] Whilst self-assembly methods are the work-horse techniques for the fabrication of molecular species on surfaces for molecular electronics, Langmuir-Blodgett technologies have been reported as a useful alternative for the preparation of directionally oriented monolayers.[35] In this paper, we make use of the LB method for the fabrication of directionally oriented monolayers of an anti-symmetric oligomeric phenylene ethynylene oligomer (OPE) derivative, namely **4-((4-((4-ethynylphenyl)ethynyl)phenyl)ethynyl)benzoic acid** (Figure 1, HOPEA). Herein we examine the capacity of the terminal alkyne moiety to serve as a contacting group for molecular electronics applications by measuring the conductivity of monomolecular layers on gold substrates using scanning tunneling microscopy (STM).

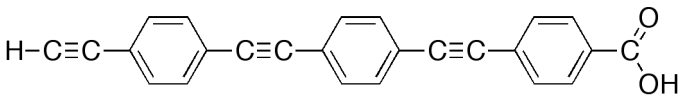

Figure 1. Molecular structure of
4-((4-((4-ethynylphenyl)ethynyl)phenyl)ethynyl)benzoic acid (HOPEA)

Experimental Section

Synthesis. See supporting information for details about the synthesis of 4-((4-((4-ethynylphenyl)ethynyl)phenyl)ethynyl)benzoic acid (HOPEA)

Films Fabrication and Characterization

The films were prepared on a Nima Teflon trough with dimensions (720x100) mm^2, which was housed in a constant temperature (20±1 ºC) clean room. A Wilhelmy paper plate pressure sensor was used to measure the surface pressure (π) of the monolayers. The sub-phase was an aqueous (Millipore Milli-Q, resistivity 18.2 MΩ·cm) solution of NaOH whose pH was 9, in which the carboxylic groups are expected to be ionized leading to a more expanded isotherm due to the repulsive Coulombic forces between the negatively charged acid moieties, which should reduce the formation of 3D aggregates at the air-water interface.[36] A solution of HOPEA in hexane:ethanol (2:1) (both solvents purchased from Aldrich and used as received; purity HPLC grade 99% and >99.5%, respectively) was delivered from a syringe held very close to the surface, allowing the surface pressure to return to a value as close as possible to zero between each addition. Hexane was employed as the spreading solvent since the HOPEA is not soluble in other common solvents used in the Langmuir-Blodgett technique (e.g. chloroform). The use of ethanol in the spreading solvent serves to limit the formation of hydrogen-bonded carboxylic acid dimers and aggregates in solution prior to deposition.[36] The spreading solvent was allowed to completely evaporate from the surface of the sub-phase over a period of at least 20 min before compression of the monolayer commenced at a constant sweeping speed of 0.015 $nm^2 \cdot molecule^{-1} \cdot min^{-1}$. Each compression isotherm was recorded at least three times to ensure the reproducibility of the results so obtained. Under the described experimental conditions the isotherms were highly reproducible. The ΔV-A measurements were carried out using a Kelvin Probe provided by Nanofilm Technologie GmbH, Göttingen, Germany. A commercial mini-Brewster angle microscope (mini-BAM) also from Nanofilm Technologie GmbH, Göttingen, Germany, was employed for the direct visualization of the monolayers at the air/water interface and a commercial UV–vis reflection spectrophotometer, details described elsewhere,[37]

was used to obtain the reflection spectra of the Langmuir films during the compression process.

The solid substrates used for the transferences were cleaned carefully as described elsewhere.[38,39] The monolayers were deposited onto cleaved mica, gold, silicon, or quartz substrates at a constant surface pressure by the vertical dipping method (the dipping speed was 3 $mm \cdot min^{-1}$). UV-vis spectra of the LB films were acquired on a Varian Cary 50 spectrophotometer and recorded using a normal incident angle with respect to the film plane. Quartz Crystal Microbalance (QCM) measurements were carried out using a Stanford Research System instrument and employing AT-cut, α-quartz crystals with a resonant frequency of 5 MHz having circular gold electrodes patterned on both sides. Atomic Force Microscopy (AFM) experiments were performed by means of a Multimode 8 AFM system from Veeco, using the tapping mode. The data were collected with a silicon cantilever provided by Bruker, with a force constant of 40 mN and operating at a resonant frequency of 300 kHz. The images were collected with a scan rate of 1 Hz, an amplitude set point lower than 1 V, and in ambient air conditions. A silicon cantilever provided by Nanoworld was used, with a force constant of 42 mN and operating at a resonant frequency of 285 kHz.

Cyclic voltammetry (CV) experiments were carried out in an electrochemical cell containing three electrodes as described before.[40] The working electrode was a gold electrode with the deposited LB film, the counter electrode was a platinum sheet, and the reference electrode was Ag|AgCl|sat'd KCl (aq.).

X-ray photoelectron spectroscopy (XPS) spectra were acquired on a Kratos AXIS ultra DLD spectrometer with a monochromatic Al Kα X-ray source (1486.6 eV) using a pass energy of 20 eV. The photoelectron take-off angle was 90 º with respect to the sample plane. To provide a precise energy calibration, the XPS binding energies were referenced to the Au($4f_{7/2}$) peak at 84.0 eV. The thickness of LB films on the gold substrates was estimated using the attenuation of the Au-4f signal from the substrate according to $I_{LB\,film} = I_{substrate} \exp(-d / \lambda \sin\theta)$,[41] where d is the film thickness, $I_{LB\,film}$ and $I_{substrate}$ are the average of the intensities of the $Au4f_{5/2}$ and $Au4f_{7/2}$ peaks attenuated by the LB film and from bare gold, respectively, θ is the photoelectron take-off angle, and λ is the effective attenuation length of the photoelectron (4.2 ± 0.1 nm).[42]

Reflectivity experiments were performed with a Bruker D8 Advance, with Cu Kα radiation (λ = 1.54 Å). Continuous scans along omega/2theta (2θ - ω) were obtained.

The reflected beam intensity was recorded as a function of the wave vector transfer along the substrate normal. The wave vector transfer (Q_z) is directly related to the incident angle, $Q_z = \sin \theta_{inc.} \times 4\pi/\lambda$. No off-specular/background scattering has been subtracted, and the intensities are given in arbitrary units because the curves have been rescaled. Simulations were carried out using *Leptos* software suite where a layered sample model was constructed to generate a simulated reflectivity curve, given the initial mass density, thickness, and interface roughness parameters. Initial parameters were refined to minimize the deviation between the experimental and simulated reflectivity curves. The simulated annealing algorithm was used in the trial-and-error process.

An Agilent STM Picoplus 2500 STM system running the Picoscan 5.3.3 software was used for the characterization of the electrical properties of the LB films. In these measurements the tip potential is referred to as U_t. STM tips were freshly prepared for each experiment by etching of a 0.25 mm Au wire (99.99%) in a mixture of HCl (50%) and ethanol (50%) at +2.4 V. Gold films employed as substrates were purchased from Arrandee®, Schroeer, Germany. These were flame-annealed at approximately 800-1000 ºC with a Bunsen burner immediately prior to use. This procedure is known to result in atomically flat Au(111) terraces.[43]

Results and Discussion

Synthesis

The preparation of HOPEA was carried out from hexyl-4-(ethynyl)benzoate in a sequential manner involving Songashira cross coupling reactions with 4-bromo(trimethylsilylethynyl)benzene, desilylation (NBu_4F) and further chain extension. The presence of the hexyl ester served to maintain sufficient solubility in the various intermediate compounds to permit facile purification by conventional column chromatography and analysis by solution spectroscopic methods. In contrast, the methyl esters were highly insoluble and far less tractable materials to work with. In the final step, the hexylester was hydrolysed with NBu_4OH, which also served to remove the trimethylsilyl protecting group. Combustion analysis of HOPEA was complicated by the formation of a thermally stable (ca. 1000 °C) material following loss of CO / CO_2 (ca. 450 °C) and acetylene (ca. 791 °C) (detected by TGA-MS). Others have noted the formation of glassy carbon materials from thermal degradation of phenylene ethynylene oligomers, and products are very likely formed from HOPEA.[44]

Fabrication and Characterization of Langmuir and Langmuir-Blodgett films

Figure 2 shows a reproducible surface pressure-area per molecule (π-A) isotherm of a HOPEA Langmuir film fabricated onto a NaOH aqueous sub-phase. The π-A isotherm is characterized by a zero surface pressure in the 1.8-0.50 $nm^2 \cdot molecule^{-1}$ range, featuring a lift-off at ca. 0.50 $nm^2 \cdot molecule^{-1}$ followed by a monotonous increase of the surface pressure upon compression. The surface potential-area per molecule (ΔV-A) isotherm is also depicted in Figure 2 for comparison purposes. The ΔV-A isotherm can often provide useful information relating to the molecular order within the monolayer, showing phase changes a few $Å^2$ before they are detected in the π-A isotherm, and this can be clearly seen in the case of the HOPEA. Compression of HOPEA monolayer results in an increase of the surface potential with this increase in ΔV being observed at higher values of the area per molecule than those corresponding to the increase in the surface pressure in the π-A isotherm. This is indicative of a progressive orientation of the molecules even in the gas phase where $\pi \rightarrow 0$. Another

especially worthy of note feature in the ΔV-A isotherm is the sudden decrease of ΔV values at ca. 0.18 nm^2 which corresponds to a surface pressure of 20 mN/m. This decrease in ΔV values upon compression is consistent with local collapses of the monolayer, in which the dipole moments are randomly distributed in a three-dimensional arrangement of HOPEA molecules. This observation is in agreement with the increase in the brightness of certain regions of Brewster angle microscopy (BAM) images at 20 mN/m (inset of Figure 2). It is important to highlight that the OPE derivative used in this work lacks the alkyl chains commonly used to stabilize films by promoting strong van der Waals interactions between neighboring molecules. Instead, it has an acetylenic (C≡C) moiety that is probably causing higher aggregation due to conjugation enhancement. This may lead to doubts about the likelihood of fabricating stable and homogeneous monolayers at the water-air interface. However, BAM images show no evidence of the formation of three dimensional aggregates under the experimental conditions used to fabricate these films.

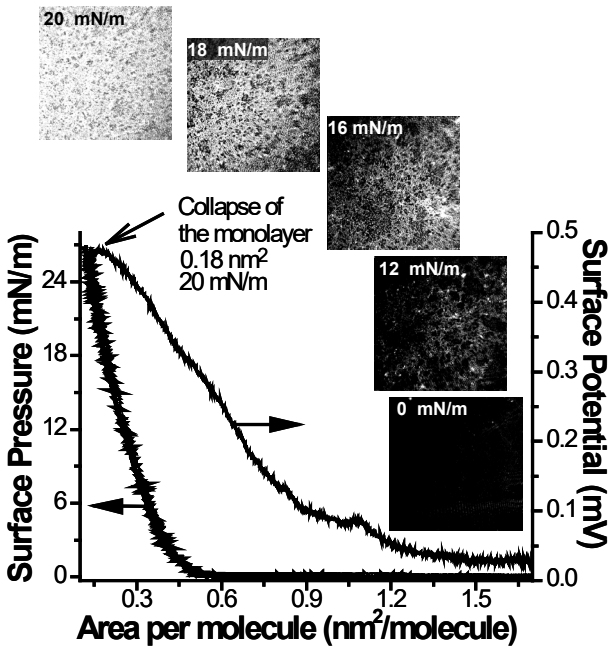

Figure 2. Surface pressure vs. area per molecule (π-A) and surface potential (ΔV-A) isotherms of HOPEA onto a NaOH aqueous sub-phase (pH = 9) at 20 ºC, and BAM images of HOPEA at the air-liquid interface at the indicated surface pressures.

Molecular orientation and two-dimensional (2D) aggregation phenomena associated with HOPEA at the air-water interface were investigated by in situ UV-vis

reflection spectroscopy through reflection of unpolarized light under normal incidence. The reflection spectra, ΔR, at different values of the area per molecule upon the compression process were recorded. Figure 3 shows the normalized spectra, $\Delta R_n = \Delta R \cdot A$ (where A is the area per molecule of HOPEA at the air-water interface at several surface pressures) together with the absorption spectrum of HOPEA in a hexane:ethanol 2:1 solution. As can be seen in Figure 3, there is a significant blue shift of the reflection spectra recorded at the air-water interface of ca. 41 nm relative to the solution spectrum. This blue shift is attributed to the formation of 2D H-aggregates as reported before for other LB films in which the chromophore has the main transition dipole arranged more or less along the amphiphile backbone, such as *trans*-stilbenes,[45,46] *trans*-azobenzenes,[47] hemicyanine derivatives,[48] tolan,[49] and other OPE derivatives.[36] The hypsochromic shift of the Langmuir film is persistent and practically independent of the applied surface pressure, which indicates that the arrangement observed in the film must represent a minimum-free-energy conformation for the system and suggests that the formation of the aggregate or assembly responsible for the blue-shifted spectroscopic profile aggregates does not depend for its formation upon orientation imposed by the LB technique. A quantitative analysis has allowed us to calculate the tilt angle of the transition dipole moment of the molecule with respect to the water surface, ϕ (inset of Figure 3).This angle was determined by comparing the reflection spectra at air-water interface and UV-vis absorption spectrum at dissolution of HOPEA. The method and relationships used to achieve these results have been comprehensively detailed elsewhere.[37] The obtained results indicate that no significant change in the tilt angle of the molecules occurs upon the compression process and this angle is slightly above 60 degrees from the beginning of the isotherm lift-off.

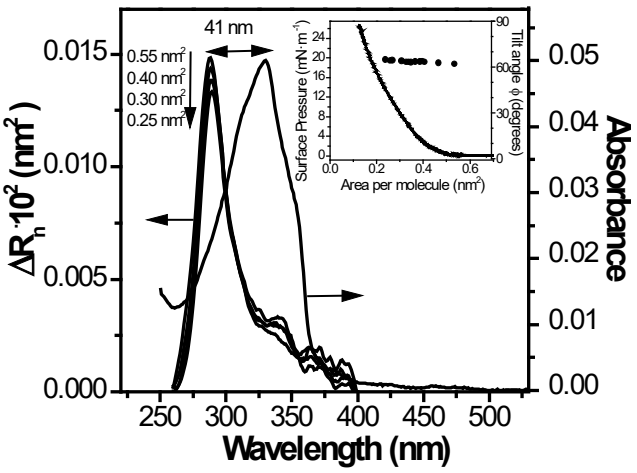

Figure 3. Normalized reflection spectra upon compression (left) and absorption spectrum of a 10^{-5} M solution of HOPEA in hexane:ethanol (right). The inset figure illustrates the variation of the tilt angle (ϕ) of the main transition dipole moment of HOPEA molecules with respect to the water surface upon the compression process.

Atomic force microscopy (AFM) was used to provide topographic images of the LB films and, thus, to check the homogeneity and quality of the films transferred onto mica substrates at different surface pressures. Representative images and section analysis profiles are shown in Figure 4. AFM images of HOPEA monolayers transferred at 18 $mN \cdot m^{-1}$ show a homogeneous surface, in which the mica is wholly covered by the monolayer. Films transferred at 15 $mN \cdot m^{-1}$ show the presence of holes on the surface. In contrast, monolayers deposited at a surface pressure of 20 $mN \cdot m^{-1}$ lead to much less homogeneous films, which are characterized by the presence of irregular domains. The film roughness, calculated in terms of the root mean squared (RMS), is 0.142 nm at 15 $mN \cdot m^{-1}$, 0.064 nm at 18 $mN \cdot m^{-1}$, and 0.415 nm at 20 $mN \cdot m^{-1}$. From these results it can be concluded that a surface pressure around 18 $mN \cdot m^{-1}$ yields very homogeneous films, which are remarkably free of defects. During the upstroke process, the deposition ratio is close to unity (≈ 1.05) for the transference surface pressure of 18 $mN \cdot m^{-1}$.

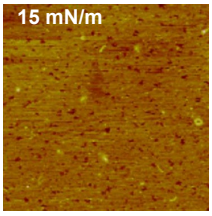

Figure 4. AFM images (left) and section analysis profile (right) of a one-layer LB film transferred onto freshly cleaved mica at the indicated surface pressures

Electrochemical electron transfer currents at electrodes under controlled potential provide an indirect measure of defect densities in thin films[50] where electron transport by tunneling through the film is significantly blockaded and can be conveniently studied by cyclic voltammetry for the film coated electrodes. Cyclic voltammograms (CV) obtained from aqueous solutions containing 1 mM $[Ru(NH)_6]Cl_3$ and 0.1 M KCl for a bare gold and for a gold working electrode modified by a one-layer LB film deposited at the indicated surface pressures of transference are shown in Figure 5. The electrochemical response of a bare gold electrode exhibits a clear voltammetric wave for the ruthenium redox probe. The significant blockade for the electrode modified by the LB film transferred at 18 $mN \cdot m^{-1}$ points to a low density of holes or defects in the monolayer. Nevertheless, the small, but clearly apparent, sigmoidal wave does indicate that there is either a certain density of defects or electron tunnelling across the film from and to the approaching electroactive redox species can occur. Higher and lower surface transference pressures give rise to much more significant voltammetric waves, indicating they offer lower blockade. These electrochemical results show that that 18 $mN \cdot m^{-1}$ is an optimum surface pressure of transference, but even at this value complete suppression of electron transfer from the gold surface to the redox probe in solution is not achieved.

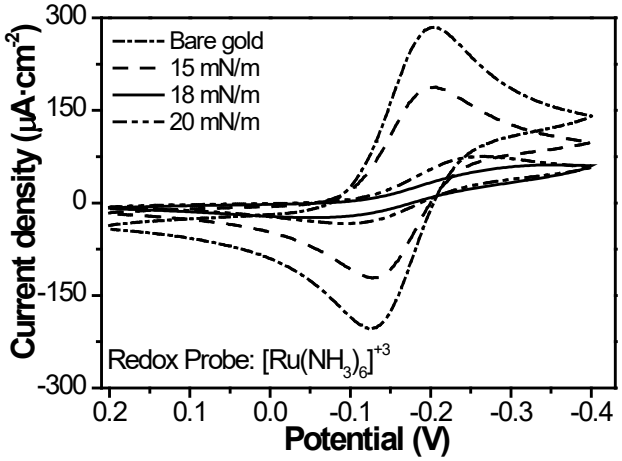

Figure 5. Cyclic voltammograms of one-layer thick LB films of HOPEA deposited on gold electrodes at different surface transference pressures. An electrochemical potential was applied to the LB films deposited on a working gold electrode immersed in aqueous solutions with 1 mM $[Ru(NH)_6]Cl_3$ and 0.1 M in KCl. The scan rate was 0.1 $V \cdot s^{-1}$ at 20

ºC. The reference electrode was Ag|AgCl|sat'd KCl and the counter electrode was a Pt sheet.

During the immersion process, the transference ratio is close to zero; therefore, the deposition of HOPEA molecules is Z-type, resulting in the formation of non-centrosymmetric LB layers, which could be of interest at a later stage for non-linear optical applications. This deposition rate was also assessed using a quartz crystal microbalance (QCM). Thus, the frequency change (Δf) for a QCM quartz resonator before and after the deposition process was determined. Taking into account the Sauerbrey equation:[51]

$$\Delta f = -\frac{2 \cdot f_0^2 \cdot \Delta m}{A \cdot \rho_q^{1/2} \cdot \mu_q^{1/2}} \quad (1)$$

where f_0 is the fundamental resonant frequency of 5 MHz, Δm(g) is the mass change, A is the electrode area, ρ_q is the density of the quartz (2.65 g·cm^{-3}), and μ_q is the shear module ($2.95 \cdot 10^{11}$ dyn·cm^{-2}), and HOPEA molecular weight (346 g·mol^{-1}), the surface coverage (Γ) is $8.7 \cdot 10^{-10}$ mol·cm^{-2}, which is in good agreement with the estimated value for the saturated surface coverage, $8.3 \cdot 10^{-10}$ mol·cm^{-2}, determined from the molecular area of HOPEA at the air-water interface at the surface pressure studied.

However, the issue of whether these films are fully organized with all the carboxylic groups attached to the substrate or a subsequent reorganization of the film occurs is not addressed by the above experiments. To further study the homogeneity of the molecular ordering and surface orientation, a quantitative study based on the different chemical reactivity of the -COOH and -C≡C-H terminal groups with an amine was undertaken (Scheme 1). The frequency change (Δf) for a QCM quartz resonator before and after the exposure of an Au-OOC-OPE-C≡C-H monomolecular film to an amine solution ($H_{13}C_6$-O-OPE-NH_2 $4.3 \cdot 10^{-4}$ M in $CHCl_3$, 4 hours) indicates that no binding of the amine to the surface film occurs since no change in the frequency was observed. In contrast, a frequency change for the QCM quartz resonator would have been observed if a certain fraction of the acetylene groups were attached to the gold substrate (which would lead to outward facing carboxylic acid groups which could bind the amine).[35] To verify the result and the significance of the consistency of the QCM results, a control experiment with behenic acid in which the alkyl chain was attached to the substrate and the acid group was the terminal free group (facing away from the surface) was undertaken. In this case, a monolayer of the amine derivative, $H_{13}C_6$-O-OPE-NH_2, was deposited onto

the behenic acid terminated LB film which gave rise to a change in the frequency of the QCM resonator. These results indicate that the QCM is sensitive enough to register the acid-base interactions with a monolayer substrate, and indicates a defined orientation of the HOPEA molecules in the films according to the deposition mode.

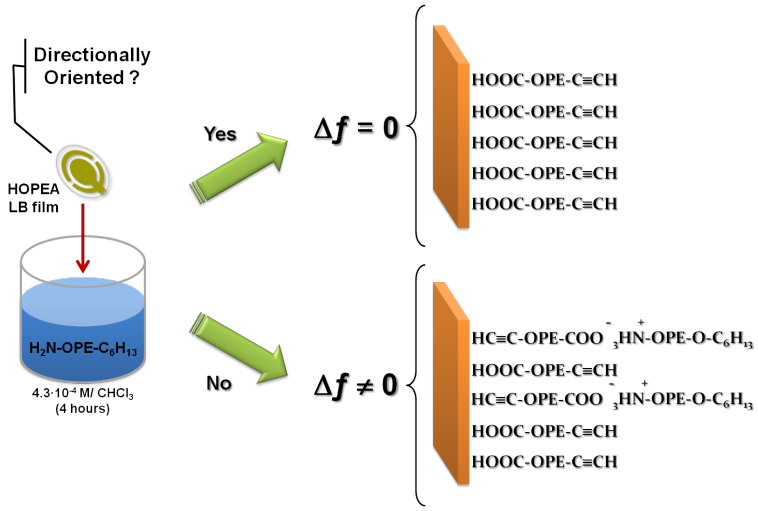

Scheme 1. A schematic showing the QCM experiment performed to probe that the obtained LB films are directionally oriented.

The optical properties of the transferred films offer additional insight into the molecular arrangement and degree of order within the film. Langmuir films of HOPEA were transferred onto quartz substrates at 18 $mN \cdot m^{-1}$ during the upstroke of the substrate and the UV-vis absorption spectrum was recorded (Figure 6). For the purpose of comparison, the UV-vis spectrum of HOPEA in hexane:ethanol solution and the reflection spectrum of the Langmuir film at 18 $mN \cdot m^{-1}$ are also plotted. The spectrum is similar in profile to the reflection spectra obtained at the air-water interface upon compression, with a maximum absorption feature at 289 nm although the spectrum of the LB film is broader which may suggest a higher aggregation. In addition, lower values in the molar absorptivity for the films in comparison with the solution are indicative of a preferential orientation of the molecules in the film with the transition dipole moment oriented in a quite vertical position with respect to the substrate or interface.

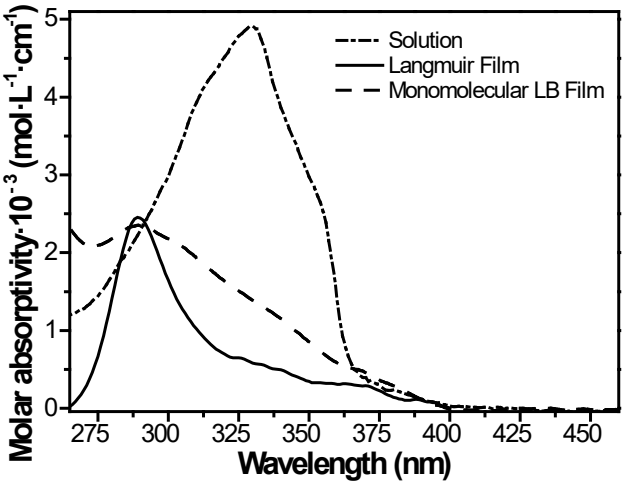

Figure 6. Molar absorptivity for a HOPEA solution in hexane:ethanol, a Langmuir film at the air-water interphase, and a monomolecular film of HOPEA transferred at 18 $mN \cdot m^{-1}$ onto a quartz substrate during the withdrawal of the substrate from the water subphase.

Si (100) substrates with one monolayer transferred at 18 $mN \cdot m^{-1}$ were analyzed with X-Ray Reflectivity (XRR). The experimental data are shown in Figure 7, expressed by reflectivity vs. momentum transfer (Q_Z) together with the fitting model. The results confirm that a uniform monolayer can be transferred onto the silicon substrate. The fitting varies the free parameters in order to achieve a match between the measured and the calculated reflectivity. A layer of SiO_2 on top of the Si(100) has been included in the simulation in order to obtain better modeling.[17] The fitting indicates that the overall thickness of the monolayer is ca. 2.04 ± 0.01 nm, while the length of the molecule in this configuration has been estimated to be 2.12 nm using molecular models (Chem3D®).

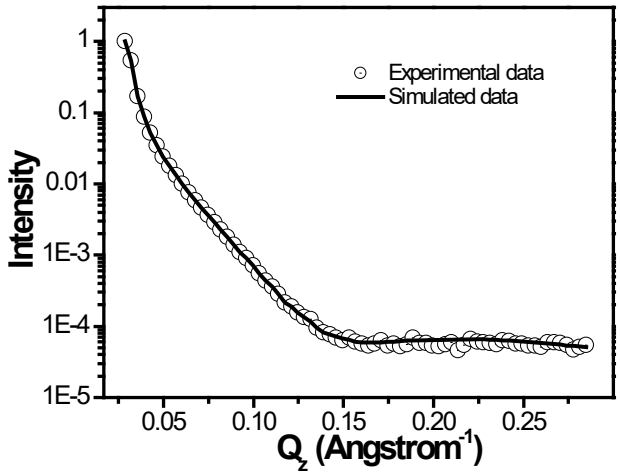

Figure 7. XRR spectrum of a single LB monolayer of HOPEA transferred onto a Si(100) substrate at a surface pressure of 18 $mN \cdot m^{-1}$:

The thickness of the monolayer was also determined using the attenuation of the Au-4f signal in the XPS spectrum as explained in the experimental section. The thickness of the film determined by this method is 2.01 ± 0.05 nm, in excellent agreement with the value calculated by the XRR technique.

Electrical properties of HOPEA LB films

The electrical properties of these LB films were determined using a scanning tunneling microscope (STM). For these STM measurements, the monolayers were deposited at 18 mN/m onto Au(111). To ensure reproducibility and reliability of the results, current-voltage (*I-V*) curves were recorded and averaged from multiple scans (720 scans) at different locations on the substrate and using different samples. Moreover, before recording *I-V* curves, it is necessary to have an estimate of the tip-to-substrate distance (*s*), in order to position the tip sufficiently above the monolayer, hence avoiding either locating the tip well above the monolayer or embedding it within the monolayer. If the STM tip is not in contact with the monolayer, the tunneling current measured represents tunneling through both the monolayer and the gap which exists between the top of the monolayer and the tip. On the other hand, if the STM tip penetrates the monolayer it is difficult to establish how far the tip penetrates and it is difficult to describe the complex contacting between tip and film and the film deformation. In order to estimate the tip-to-film proximity it is necessary to know both the thickness of the monolayer and the tip-to-substrate distance (*s*). The thickness of the monolayer (2.01 ±0.05) nm, was determined by using the attenuation of the Au4f signal in the XPS spectra as explained before. Tip-to-substrate distance was estimated by relating the set-point parameters ($I_0 \equiv$ "set-point current" and $U_t \equiv$ "tip bias") to an estimated gap separation by using a distance calibration procedure. For conditions where the tip is embedded within the film, current-distance scans which display a monotonic exponential decrease of the tunneling current as the tip is retracted were recorded at regular intervals during the measurements. These monotonic exponential decay curves were then plotted as ln(*I*) versus *s*. Averaging the slope of the corresponding $d\ln(I)/ds$ curves yields $d\ln(I)/ds$ values typically on the order of (5.46 ±

0.97) nm^{-1}. This d$\ln(I)$/ds value corresponds to an average current "decay value" within the film. It is then assumed that the conductance at the point where metal-tip contact occurs is the conductance quantum G_0 ($G_0 = 2e^2/h \approx 77.4$ μS). These values can then be used in conjuction with the equation below as the basis for an estimation of the tip-to-distance at a given current:

$$s = \frac{\ln\left(G_0 \times U_t / I_0\right)}{d\ln(I)/ds} \qquad (2)$$

Figure 8.a shows *I-V* curves obtained for a one layer LB film transferred onto Au(111) at 18 mN/m using several set-point parameters: U_t = 0.6 V and I_0 = 0.5, 0.8, and 1.1 nA which give a tip-to-substrate distance of 2.09, 2.01 and 1.95 nm, respectively according to Equation 2. Since the independently determined thickness of the monolayer is (2.01 ± 0.05) nm, when using the set-point parameters of 0.6 V and 0.8 nA the STM tip is estimated as being located just above the monolayer. Meanwhile, for 1.1 nA (s = 1.95 nm) the tip penetrates inside the monolayer (conductance increases) and for 0.5 nA (s = 2.09 nm) there is a notable gap between the tip and the LB film (junction conductance decreases).

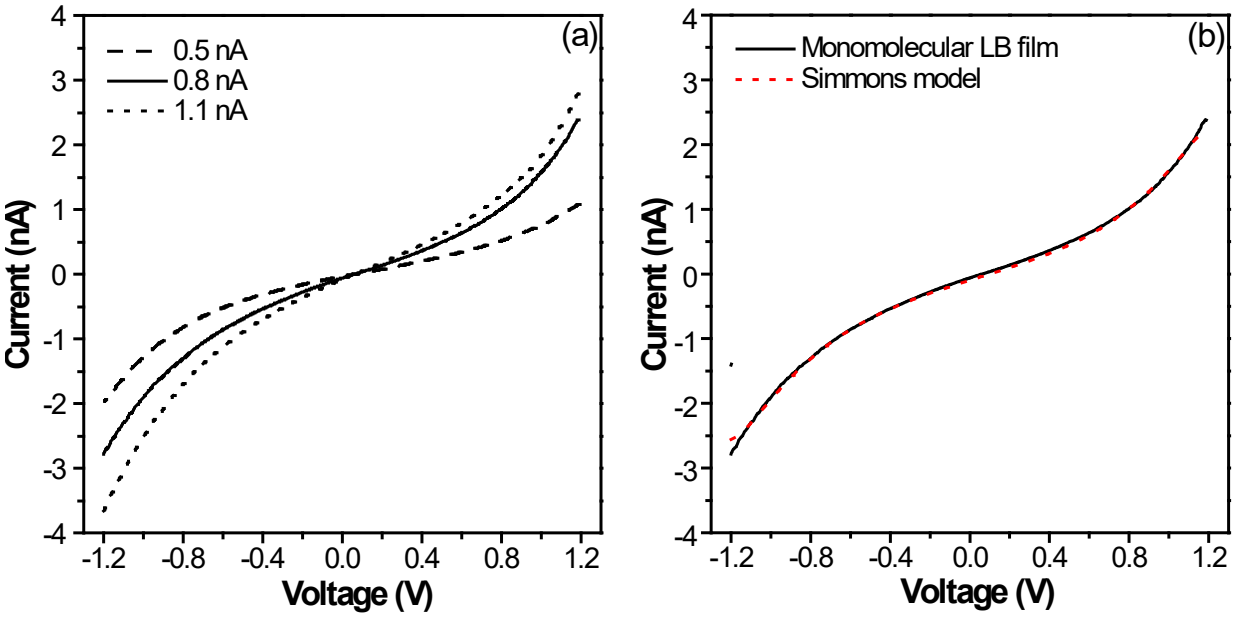

Figure 8. a) *I–V* curves of a monomolecular LB film of HOPEA transferred onto Au(111) at 18 mN·m^{-1} using several set-point parameters: 0.5 nA (s=2.09 nm); 0.8 nA (s=2.01 nm); and 1.1 nA (s=1.95 nm). U_t = 0.6 V. b) *I–V* curve of a monomolecular LB film of HOPEA at 0.8 nA and fitting according to the Simmons equation, Φ = 0.68 eV, and α = 0.42.

The *I-V* response obtained at 0.8 nA is close to ohmic between bias voltages of -0.6 to +0.6 V giving a molecule conductance value of ca. (1.48×10^{-5}) G_0. This value is of the same order of magnitude as the conductance values obtained for other OPE derivatives using different functional groups as anchoring groups to make the contact with the metal, even at both ends of the molecule.[17,35,52] This leads us to conclude that the π-electron rich triple bonds of acetylenic end groups can be used as effective linkers in metal-molecule-metal junctions and that they do not appear to notably attenuate the electronic transmission when compared to other linkers (e.g. –SH, -COOH, NH_2). This demonstrates that acetylenic end groups are alternative anchoring groups in such junctions and that show comparably effective electronic coupling at metal-molecule contacts. In addition, acetylenic moieties can be used to further modify the molecular species within the junction by facile click chemistry methods.[53,54] Outside the -0.6 to +0.6 voltage range the response clearly deviates from linearity showing a sigmoidal behavior over the full voltage region, in accordance with the Simmons model fitting (see below). However, the *I-V* curves are relatively symmetrical despite the asymmetry of the molecule. This implies that its behavior is like that of a molecular wire where the molecule is simply an amphiphilic electron-donating wire, as has been previously reported for similar "anti-symmetric" OPE derivatives,[16,17,35,55] and does not behave like a molecular diode with strong rectifying characteristic produced by the asymmetric molecular junction.

The *I-V* curve characteristics (sigmoidal *I-V* curve and absence of any spectroscopic peaks in the *I-V* curve) points towards a non-resonant tunneling mechanism of transport through these metal-molecule-metal junctions. One of the simplest tunneling barrier models that can be used for comparison with the experimental *I-V* data is the Simmons model.[56] In this model, the current *I* is given by:

$$I = \frac{Ae}{4\pi^2 \hbar s^2}\left\{\left(\Phi - \frac{eV}{2}\right)\exp\left[-\frac{2(2m)^{1/2}}{\hbar}\alpha\left(\Phi - \frac{eV}{2}\right)^{1/2}s\right] - \left(\Phi + \frac{eV}{2}\right)\exp\left[-\frac{2(2m)^{1/2}}{\hbar}\alpha\left(\Phi + \frac{eV}{2}\right)^{1/2}s\right]\right\} \quad (3)$$

where V is the applied potential, A is the contact area of the molecule with the tip (0.20 nm^2 in concordance to the isotherm shown in Figure 2 at the surface pressure of 18 $mN \cdot m^{-1}$), s is the width of the tunneling barrier which was assumed to be the through-bond distance between the end groups (carboxylic acid and acetylene) in OPE molecular wire as calculated with a molecular modeling program (2.12 nm), Φ is the effective

barrier height of the tunneling junction (relative to the Fermi level of the Au), α is related to the effective mass of the tunneling electron and *m* and *e* represent the mass and the charge of an electron. To fit the *I-V* data in Figure 8.b,Φ and α are the fit parameters. A good agreement between the data and the model is obtained with Φ = 0.67 eV, and α = 0.37. This effective barrier height is rather similar or even lower than that obtained for either "symmetric" OPEs with amine ($\Phi \sim 0.60$ eV)[57] or thiol groups ($\Phi = 0.77$ eV)[58] at both ends of the molecule or for "asymmetric" OPEs using different end groups.[17,35] Therefore, we conclude from these collected electrical measurements, that terminal acetylene moieties can function as linkers, suitable for coupling conjugated molecular backbones to gold terminals. Single molecule conductance values obtained here for OPEs with acetylenic end groups are comparable to those using more conventional chemisorption chemistry (e.g. –SH, -COOH, NH_2) between the gold contacts and the molecule. In addition, since Equation 3 is based on a very simple model of non-resonant tunneling and gives a good description of our experimental *I-V* data, it is reasonable to assume that the mechanism of transport through these metal-molecule-metal junctions is non-resonant tunneling.

Conclusions

An "antisymmetric" OPE derivative, with an acid group at one terminus of the molecule and an acetylene group linked to the aromatic ring at the other, has been synthesized and assembled into well-packed monolayer films by means of the Langmuir–Blodgett technique. Langmuir films were prepared at the air-water interface and characterized by surface pressure vs. area per molecule isotherms and Brewster angle microscopy, which revealed that this molecule can form true monomolecular films at the air-water interface. These monomolecular films were transferred undisturbed onto solid substrates with a transfer ratio close to 1 with a Z-type deposition. QCM experiments demonstrated that HOPEA was linked through the acid group to the gold substrate. Atomic force microscopy images together with cyclic voltammetry experiments revealed the formation of highly homogeneous films with low defect densities at an optimized transfer surface pressure of 18 $mN \cdot m^{-1}$. Electrical characteristics of the LB films on gold substrates were determined, obtained by recording *I-V* curves with a gold STM tip positioned just above the monolayer (as

determined from calibration of the tip-to-substrate distance and knowledge of the thickness of the LB film determined from XPS measurements). *I-V* curves were symmetric, despite "anti-symmetric" contacting of the molecule junction with respect to the tip and the substrate. These *I-V* curves and good Simmons model fits indicate that charge flow through the HOPEA metal-molecule-metal junction is via a non-resonant tunnelling mechanism. Importantly, it is concluded that the acetylene group is an efficient anchoring group, which provides effective electronic coupling at metal-molecule contacts. Finally, the terminal acetylene group at the LB monolayer additionally raises the prospect of chemically anchoring gold nanoparticles or even a second layer, of a different compound, to the monolayer, thereby offering a new route to the construction of well-defined sandwich-type structures.

Acknowledgments

L.M.B., S.M., M.C.L., and P.C. are grateful for financial assistance from Ministerio de Ciencia e Innovación from Spain and fondos FEDER in the framework of projects CTQ2009-13024 and MAT2010-10846-E. P.J.L holds an EPSRC Leadership Fellowship. R.J.N. thanks EPSRC for funding. S.M. acknowledges his Juan de la Cierva position from Ministerio de Ciencia e Innovación (Spain) and L.M.B acknowledges her grant from Banco Santander.

Supporting Information Available: Full description of the material. This material is available free of charge via the Internet at http://pubs.acs.org.

References

(1) Aviram, A.; Ratner, M. *Chem. Phys. Lett.* **1974**, *29*, 277-283.
(2) Donoli, A.; Bisello, A.; Cadena, R.; Ceccon, A.; Bassetti, M.; D'Annibale, A.; Pasquini, C.; Raneri, A.; Santi, S. *Inorg. Chim. Acta* **2011**, *374*, 422-446.
(3) Yee, S. K.; Sun, J. B.; Darancet, P.; Tilley, T. D.; Majumdar, A.; Neaton, J. B.; Segalman, R. A. *ACS Nano* **2011**, *5*, 9256-9263.
(4) Yao, J.; Li, Y.; Aou, Z.; Yang, J.; Yin, Z. *Physica B: Condensed Mater* **2011**, *406*, 3969-3974.
(5) Fuentes, N.; Martin-Lasanta, A.; de Cienfuegos, L. A.; Ribagorda, M.; Parra, A.; Cuerva, J. M. *Nanoscale* **2011**, *3*, 4003-4014.

(6) Cao, Y.; Steigerwald, M. L.; Nuckolls, C.; Guo, X. *Adv. Mater.* **2010**, *22*, 20-32.
(7) Beebe, J. M.; Engeelkes, V. B.; Miller, L. L.; Frisbie, C. D. *J. Am. Chem. Soc.* **2002**, *124*, 11268-11269.
(8) Kamenetska, M.; Koentopp, M.; Whalley, A. C.; Park, Y. S.; Steigerwald, M. L.; Nuckolls, C.; Hybertsen, M. S.; Venkataraman, L. *Phys. Rev. Lett.* **2009**, *102*, 126803-126804.
(9) Ko, C.; Huang, M.; Fu, M.; Chen, C. *J. Am. Chem. Soc.* **2010**, *132*, 756-764.
(10) Mishchenko, A.; Zotti, L. A.; Conlanthen, D.; Bulrkle, M.; Pauly, F.; Cuevas, J. C.; Mayor, M.; Wandlowski, T. *J. Am. Chem. Soc.* **2011**, *133*, 184-187.
(11) Martin, S.; Grace, I.; Bryce, M. R.; Wang, C. S.; Jitchati, R.; Batsanov, A. S.; Higgins, S.; Lambert, C. J.; Nichols, R. J. *J. Am. Chem. Soc.* **2010**, *132*, 9157-9164.
(12) Kim, B.; Choi, S. H.; Zhu, X.-; Frisbie, C. D. *J. Am. Chem. Soc.* **2011**, *133*, 19864-19877.
(13) Nichols, R. J.; Haiss, W.; Higgins, S. J.; Leary, E.; Martin, S.; Bethell, D. *Phys. Chem. Chem. Phys.* **2010**, *12*, 2801-2815.
(14) Venkataraman, L.; Klare, J. E.; Tam, I. W.; Nuckolls, C.; Hybertsen, M. S.; Steigerwald, M. N. *Nano Lett.* **2006**, *6*, 458-462.
(15) Paulsson, M.; Krag, C.; Frederiksen, T.; Brandbyge, M. *Nano Lett.* **2009**, *9*, 117-121.
(16) Villares, A.; Pera, G.; Martin, S.; Nichols, R. J.; Lydon, D. P.; Applegarth, L.; Beeby, A.; Low, P. J.; Cea, P. *Chem. Mater.* **2010**, *22*, 2041-2049.
(17) Pera, G.; Martin, S.; Ballesteros, L. M.; Hope, A. J.; Low, P. J.; Nichols, R. J.; Cea, P. *Chem. Eur. J.* **2010**, *16*, 13398-13405.
(18) Kim, Y.; Hellmuth, T. J.; Bulrkle, M.; Pauly, F.; Scheer, E. *ACS Nano* **2011**, *5*, 4104-4111.
(19) Richter, L. J.; Yang, C. S.-C.; Wilson, P. T.; Hacker, C. A.; van Zee, R. D.; Stapleton, J. J.; Allara, D. L.; Yao, Y.; Tour, J. M. *J. Phys. Chem. B* **2004**, *108*, 12547-12559.
(20) Tour, J. M.; Jones II, L.; Pearson, D. L.; Lamba, J. J. S.; Burgin, T. P.; Whitesides, G. M.; Allara, D. L.; Parikh, A. N.; Atre, S. V. *J. Am. Chem. Soc.* **1995**, *117*, 9529-9534.
(21) Stapleton, J. J.; Daniel, T. A.; Uppili, S.; Carbarcos, O. M.; Naciri, J.; Shashidhar, R.; Allara, D. L. *Langmuir* **2005**, *21*, 11061-11070.
(22) Ramachandran, G. K.; Hopson, T. J.; Rawlett, A. M.; Nagahara, L. A.; Primak, A.; Lindsay, S. M. *Science* **2003**, *300*, 1413-1416.
(23) Yasuda, S.; Yoshida, S.; Sasaki, J.; Okutsu, Y.; Nakamura, T.; Taninaka, A.; Takeuchi, O.; Shigekawa, H. *J. Am. Chem. Soc.* **2006**, *128*, 7746-7747.
(24) Kim, B.; Beebe, J. M.; Jun, Y.; Zhu, X. Y.; Frisbie, C. D. *J. Am. Chem. Soc.* **2006**, *128*, 4970-4971.
(25) Venkataraman, D.; Park, Y. S.; Whaley, A. C.; Nuckolls, C.; Hybertsen, M. S.; Steigerwald, M. L. *Nano Lett.* **2007**, *7*, 502-506.
(26) Martín, S.; Haiss, W.; Higgins, S. J.; Cea, P.; Lopez, M. C.; Nichols, R. J. *J. Phys. Chem. C* **2008**, *112*, 3941-3948.
(27) Wang, C.; Batsanov, A. S.; Bryce, M. R.; Martin, S.; Nichols, R. J.; Higgings, S. J.; Garcia-Suarez, V. M.; Lambert, C. J. *J. Am. Chem. Soc.* **2009**, *131*, 15647-15654.
(28) Martin, S.; Haiss, W.; Higgins, S. J.; Nichols, R. J. *Nano Lett.* **2010**, *10*, 2019-2023.
(29) Buschbeck, R.; Low, P. J.; Lang, H. *Coord. Chem. Rev.* **2011**, *255*, 241-272.

(30) Maity, P.; Tsunoyama, H.; Yamauchi, M.; Xie, S.; Tsukuda, T. *J. Am. Chem. Soc.* **2011**, *133*, 17142-17145.
(31) Tao, F.; Xu, G. Q. *Chem. Res.* **2004**, *37*, 882-893.
(32) Stewart, M. P.; Buriak. *J. Am. Chem. Soc.* **2001**, *123*, 7821-7830.
(33) Binder, W. H.; Sachsenhofer, R. *Macromolecular Rapid Communications* **2007**, *28*, 15-54.
(34) Kushmerik, J. G.; Whitaker, C. M.; Pollack, S. K.; Schull, T. L.; Ranganathan, S. *Nanotechnology* **2004**, *15*, S489-S493.
(35) Ballesteros, L. M.; Martín, S.; Pera, G.; Schauer, P. A.; Kay, N. J.; Lopez, M. C.; Low, P. J.; Nichols, R. J.; Cea, P. *Langmuir* **2011**, *27*, 3600-3610.
(36) Villares, A.; Lydon, D. P.; Porrès, L.; Beeby, A.; Low, P. J.; Cea, P.; Royo, F. M. *J. Phys. Chem. B* **2007**, *111*, 7201-7209.
(37) Cea, P.; Martín, S.; Villares, A.; Möbius, D.; López, M. C. *J. Phys. Chem. B* **2006**, *110* 963-970.
(38) Cea, P.; Lafuente, C.; Urieta, J. S.; López, M. C.; Royo, F. M. *Langmuir* **1996**, *12*, 5881-5887.
(39) Martín, S.; Cea, P.; Lafuente, C.; Royo, F. M.; López, M. C. *Surf. Sci.* **2004**, *563*, 27.
(40) Cea, P.; Lafuente, C.; Urieta, J. S.; López, M. C.; Royo, F. M. *Langmuir* **1997**, 4892-4897.
(41) Liu, K.; Li, G. R.; Wang, X. H.; Wang, F. S. *J. Phys. Chem. C.* **2008**, *122*, 4342-4349.
(42) Bain, C. D.; Whitesides, G. M. *J. Phys. Chem.* **1989**, *93*, 1670-1673.
(43) Haiss, W.; Lackey, D.; Sass, J. K.; Besocke, K. H. *J. Chem. Phys.* **1991**, *95*, 2193-2196.
(44) Stephens, E. B.; Tour, J. M. *Adv. Mater.* **1992**, *4*, 570-572.
(45) Kaji, H.; Shimoyama, Y. *Jpn. J. Appl. Phys.* **2001**, *40*, 1396-1400.
(46) Martin, S.; Cea, P.; Pera, G.; Haro, M.; López, M. C. *J. Colloid Interface Sci.* **2007**, *308*, 239-248.
(47) Pedrosa, J. M.; Martín, M. T.; Camacho, L.; Möbius, D. *J. Phys. Chem. B* **2002**, *106*, 2583-2591.
(48) Heesemann, J. *J. Am. Chem. Soc.* **1980**, *102*, 2167-2176.
(49) Pera, G.; Villares, A.; López, M. C.; Cea, P.; Lydon, D. P.; Low, P. J. *Chem. Mater.* **2007**, *19*, 857-864.
(50) Porter, M. D.; Bright, T. B.; Allara, D. L.; Chidsey, C. E. D. *J. Am. Chem. Soc.* **1987**, *109*, 3559.
(51) Sauerbrey, G. *Z. Physik* **1959**, *155*, 206-222.
(52) Lee, K.; Cho, S.; Park, S. H.; Heeger, A. J.; Lee, C. W.; Lee, S. H. *Nature* **2006**, *441*, 65-68.
(53) Luo, L.; Frisbie, D. *J. Am. Chem. Soc.* **2010**, *132*, 8854-8855.
(54) Ciampi, S.; Böcking, T.; Kilian, K. A.; James, M.; Harper, J. B.; Gooding, J. J. *Langmuir* **2007**, *23*, 9320-9329.
(55) Ashwell, G. J.; Urasinska, B.; Tyrrell, W. D. *Phys. Chem. Chem. Phys.* **2006**, *8*, 3314-3319.
(56) Simmons, J. G. *J. Appl. Phys.* **1963**, *281*, 1793-1803.
(57) Lu, Q.; Liu, K.; Zhang, H.; Du, Z.; Wang, X.; Wang, F. *ACS Nano* **2009**, *3*, 3861-3868.
(58) Liu, K.; Wang, X.; Wang, F. *ACS Nano* **2008**, *2*, 2315-2323.

TOC

Acetylene as a new linker: 4-((4-((4-ethynylphenyl)ethynyl)phenyl)ethynyl)benzoic acid has been assembled into well-packed monomolecular films by means of the Langmuir-Blodgett technique. The acetylene terminal group is demonstrated to be an efficient binding group suitable for construction of metal-molecule-metal junctions, making this group an interesting alternative to the more conventionally used thiol contacting chemistry for molecular wires.